Stabilizing Polyether Electrolyte with a 4 V Metal Oxide Cathode by Nanoscale Interfacial Coating

Haowei Zhai,[†,||] Tianyao Gong,[†,||] Bingqing Xu,[†,§,||] Qian Cheng,[†] Daniel Paley,[‡] Boyu Qie,[†] Tianwei Jin,[†] Zhenxuan Fu,[†] Laiyuan Tan,[†] Yuan-Hua Lin,[§] Ce-Wen Nan,[§] and Yuan Yang*[,†]

[†]Program of Materials Science and Engineering, Department of Applied Physics and Applied Mathematics and [‡]Columbia Nano Initiative, Columbia University, New York, New York 10027, United States

[§]State Key Laboratory of New Ceramics and Fine Processing, School of Materials Science and Engineering, Tsinghua University, Beijing 100084, P. R. China

S Supporting Information

ABSTRACT: Safety is critical to developing next-generation batteries with high-energy density. Polyether-based electrolytes, such as poly(ethylene oxide) and poly(ethylene glycol) (PEG), are attractive alternatives to the current flammable liquid organic electrolyte, since they are much more thermally stable and compatible with high-capacity lithium anode. Unfortunately, they are not stable with 4 V $Li(Ni_xMn_yCo_{1-x-y})O_2$ (NMC) cathodes, hindering them from application in batteries with high-energy density. Here, we report that the compatibility between PEG electrolyte and NMC cathodes can be significantly improved by forming a 2 nm Al_2O_3 coating on the NMC surface. This nanoscale coating dramatically changes the composition of the cathode electrolyte interphase and thus stabilizes the PEG electrolyte with the NMC cathode. With Al_2O_3, the capacity remains at 84.7% after 80 cycles and 70.3% after 180 cycles. In contrast, the capacity fades to less than 50% after only 20 cycles in bare NMC electrodes. This study opens a new opportunity to develop safe electrolyte for lithium batteries with high-energy density.

KEYWORDS: poly(ethylene oxide), atomic layer deposition, battery safety, polymer electrolyte, thermal runaway, lithium anode, NMC cathode
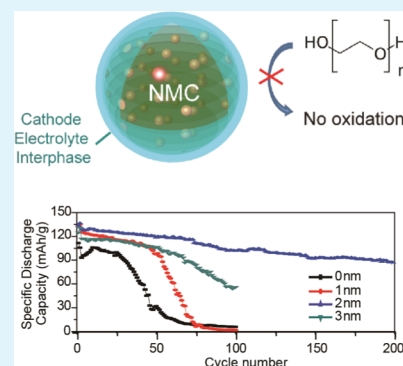
INTRODUCTION

Lithium-based rechargeable batteries with high-energy density are highly attractive for applications ranging from portable electronics to electric vehicles and grid-level energy storage.[1−9] However, higher-energy density is typically accompanied by lower thermal stability and higher safety risk.[10−15] One intrinsic and critical safety issue in lithium-based batteries is the flammability of liquid organic carbonate electrolyte, which has a low flash point around room temperature.[16] Although ionic liquids and fluorinated liquid electrolytes have shown potential to be nonflammable, their costs are high for large-scale production.[17−22]

Poly(ethylene oxide) (PEO) or poly(ethylene glycol) (PEG)-based electrolytes are attractive to address this issue on thermal stability, as they have much higher flash points (e.g., >150−200 °C, Figure S1, Supporting Information Video S1) and are compatible with state-of-the-art techniques for industrial manufacturing.[23−29] Unfortunately, PEO is a type of polyether and easily oxidized above 4.0 V vs Li/Li^{+} so that it is traditionally considered to be only compatible with LiFePO₄ with lower-energy density but not 4 V $Li(Ni_xMn_yCo_{1-x-y})O_2$ electrode materials with high-energy density.[4,30] Although various reports have shown anodic stability beyond 4.5 V vs Li/Li^{+} in cyclic voltammetry tests with stainless steel

electrodes,[26,31−33] most full-cell tests are with LiFePO₄, except few with $LiMn_{1-x}Fe_xPO_4$.[27] In contrast, LiCoO₂/PEO/Li cells show fast capacity decay, even with polymeric protection on the surface.[34] This suggests that the Ni/Co-rich surface of $Li(Ni_xMn_yCo_{1-x-y})O_2$ (NMC) catalyzes the oxidation reaction of PEO and accelerates its degradation. Therefore, we hypothesize that the effective passivation of NMC will reduce the surface's activity toward PEO oxidation, and its cycling performance can be stabilized.

In this report, a 2 nm Al_2O_3 coating is formed on the $Li(NiMnCo)_{1/3}O_2$ (NMC) electrode by atomic layer deposition (ALD) to passivate the surface, and the as-coated electrode shows significantly improved stability with short-chain poly(ethylene glycol) electrolyte (molecular weight M_w of 500, Figure 1A). When cycled between 4.2 and 2.8 V vs Li/Li^{+}, a specific capacity of 128.5 mAh/g is achieved at C/3 with a capacity retention of 84.7% over 80 cycles and 70.3% over 180 cycles at room temperature, showing significantly improved stability compared to bare NMC cathodes. The results suggest that a high-quality cathode electrolyte
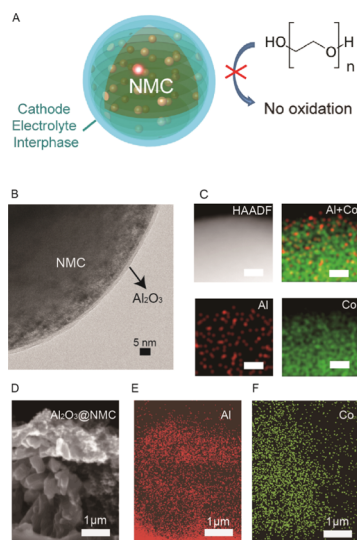
Figure 1. Design of cathode electrolyte interphase coating to suppress the oxidation of polyether-based electrolyte and stabilize the NMC cathode. (A) Schematic to illustrate the concept of protection. (B) Bright-field image of an NMC electrode with a 2 nm Al_2O_3 coating by atomic layer deposition (ALD). (C) High-angle annular dark-field image of an NMC electrode with a 2 nm Al_2O_3 coating by ALD and energy-dispersive spectroscopy (EDS) mapping of Al/Co overlapping, Al and Co. Scale bars are 5 nm. (D) Scanning electron microscope (SEM) image of the side view of an NMC electrode after 50 cycles. The bottom part is the Al current collector. (E, F) EDS mapping of (E) Al and (F) Co in (D).

interphase (CEI) is critical to stabilize a PEO-based electrolyte with the NMC cathode, which leads to new opportunity to develop safe rechargeable lithium batteries with high-energy density.

RESULTS AND DISCUSSION

In our experiments, the NMC electrode is prepared by mixing NMC, carbon black, and poly(vinylidene difluoride) (PVDF) in a ratio of 88:5:7 and doctor-bladed onto an Al foil. ALD coating is performed on the as-prepared NMC electrode by alternating water and trimethyl aluminum sources in a 4 in. ALD chamber. To allow precursors fully penetrating the torturous battery electrode, a 5 s holding period is inserted

between precursor pulse (0.03 s) and pumping (30 s). The existence of ALD Al_2O_3 coating is clearly shown in the high-angle annular dark-field (HAADF) image in scanning transmission electron microscopy (STEM) (Figure 1C), where a 2 nm amorphous coating presents on the NMC surface, and EDS mapping shows that the coating layer is Al_2O_3, indicated by the concentrated Al signal (Figure 1C). The comparison of Al with Ni, Mn, and Co at another location can be found in Figure S3. The uniform coating of Al_2O_3 through the whole electrode is further supported by energy-dispersive spectrometer (EDS) mapping in scanning electron microscope (SEM), as Al can be detected everywhere. As shown in Figure 1F, the overlapping of Co and Al in EDS mapping indicates that Al_2O_3 coating is uniform through the entire electrode. The corresponding spectrum over a large area is shown in Figure S3G, where a clear peak of Al can be seen.

To evaluate the effectiveness of such oxide coating, the as-coated NMC electrode is combined with poly(ethylene glycol) dimethyl ether (PEGDME) with an M_w of 500 and a binary salt of 0.6 M lithium bis(trifluoromethanesulfonyl)imide (LiTFSI) and 0.4 M lithium bis(oxalato)borate (LiBOB). The reason to choose such small M_w is to increase the electrolyte conductivity, which reaches 1.1×10^{-3} S/cm at 30 °C and 3.4×10^{-3} S/cm at 60 °C (Figure S4). Meanwhile, as the chemical nature of PEGDME and PEO with higher molecular weights is the same, the low M_w should have little effect on electrochemical/chemical reactions between NMC and the electrolyte, and our conclusion that Al_2O_3 coating can stabilize such a polyether electrolyte with a 4 V NMC cathode should not change. For simplicity, we will use the abbreviation PEG instead of PEGDME with an M_w of 500 in this article. The dual-salt combination of LiBOB and LiTFSI is selected as it can help prevent Al substrate from the corrosion of LiTFSI.[35−37]

The electrochemical performance of such Al_2O_3-coated NMC/PEG-LiTFSI-LiBOB/Li cell is first tested by galvanostatic cycling. After two cycles at C/10, the cell is charged at C/3 (1C = 150 mA/g), followed by a CV step down to C/20, and discharged at C/3. Both ranges of 2.8−4.2 and 2.8−4.25 V are tested. In the 2.8−4.2 V range, it is clear that the cycling stability is greatly enhanced with ALD coating, as reflected by both voltage profile (Figure 2A−D), capacity retention (Figure 2E), and Coulombic efficiency (Figure 2F). Without the
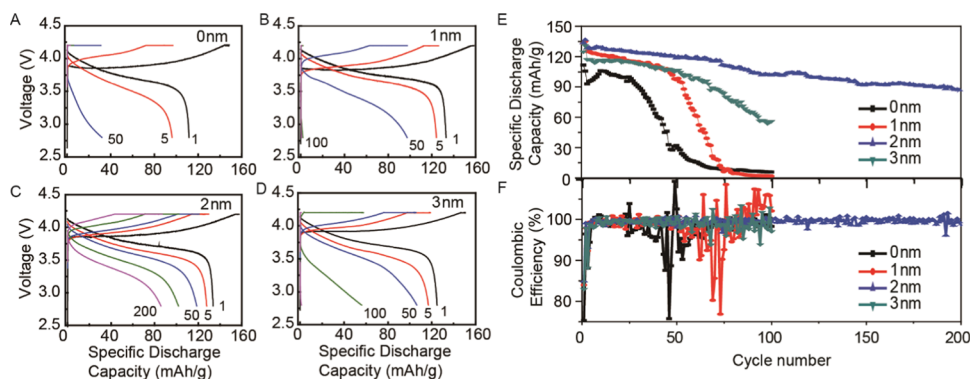
Figure 2. Electrochemical performance of bare and Al_2O_3-protected $Li(NiMnCo)_{1/3}O_2$ (NMC) electrodes. (A−D) Voltage profiles of NMC electrode at different cycles (A) without Al_2O_3 coating, (B) with a 1 nm Al_2O_3 coating, (C) with a 2 nm Al_2O_3 coating, and (D) with a 3 nm Al_2O_3 coating. (E) Cycling performance of NMC electrodes with 0, 1, 2, and 3 nm Al_2O_3 coatings. (F) Corresponding Coulombic efficiency of NMC electrodes in (D). Cells in (A)−(E) are cycled at C/3 between 4.2 and 2.8 V (1C = 150 mA/g). A constant voltage step is added at the end of charging with a current cutoff of C/20.

coating, the initial capacity at C/3 is 130.1 mAh/g but drops fast to 26.3 mAh/g after only 40 cycles (Figure 2E). Improvement can already be seen in 1 nm coating but not very effective. The initial capacity at C/3 is 125.1 mAh/g and remains at 108.3 mAh/g after 40 cycles. However, the capacity decays fast between the 50th and 80th cycles and is below 10 mAh/g at the 100th cycle. In contrast, with 2 nm coating, the initial capacity at C/3 reaches 128.5 mAh/g and maintains as high as 101.8 mAh/g after 100 cycles and 85.7 mAh/g at the 200th cycle. This represents a capacity retention of 66.7% after 200 cycles or a loss of only 0.021% per cycle. On the other hand, such a trend does not continue for 3 nm coating, where the capacity retention is only 46.0% after 100 cycles, from 117.4 mAh/g at the first cycle to 54 mAh/g at the 100th cycle. It is unclear why 3 nm coating not only decreases cell capacity but also leads to worse cycling life after 50 cycles. One possible reason is that it is easier to form regions with high impedance in samples with 3 nm coating, since the resistance of Al_2O_3 coating is very sensitive to its thickness and particles expand and contract during charge and discharge. This needs further investigation and will be studied in the future.

Such improved performance clearly validates our hypothesis that a high-quality CEI can passivate the NMC surface and suppress the oxidation of PEG electrolytes. This is further confirmed by the stabilized Coulombic efficiency (CE) for samples with Al_2O_3 coating. First, the initial CE increases slightly from 83.0% at 0 nm to 84.0% at 1 nm and 84.9% at a 2 nm Al_2O_3 coating and then goes back to 83.0% at 3 nm; the average CE in the first 100 cycles at C/3 also improves from 98.10% for 0 nm to 98.60% for 1 nm, 99.43% for 2 nm coating and 99.0% for 3 nm. Moreover, a strong correlation is also observed between the onset of fast capacity fading and the destabilization of CE. Once CE starts to fluctuate, such as the 16th cycle for bare NMC and the 50th cycle for 1 nm coating, the capacity starts to fade quickly. This suggests that the fast capacity fading in samples without Al_2O_3 protection is induced by side reactions between NMC and the PEG electrolyte.

The power capability of the 2 nm Al_2O_3-coated NMC electrodes is further evaluated for the range of 2.8−4.2 V vs Li/Li+. The specific capacities at 0.3, 0.5, and 1C are 118.8, 116.9, and 98.8 mAh/g, respectively, which are 86.3, 85.0, and 71.8% of that at 0.1C (137.6 mAh/g), as shown in Figure S5. These results are reasonable for wide applications, and the lower discharge capacity at 1C is likely a result of excessive resistance induced by the ALD coating, which can be further engineered to reduce resistance.

A similar trend of enhanced cycling stability is also observed when the cell is cycled between 2.8 and 4.25 V (Figure S6). Without the coating, the initial capacity is 135.0 mAh/g but drops fast to 19.3 mAh/g after 50 cycles. In contrast, with 2 nm coating, the initial capacity reaches 141.2 mAh/g and maintains at 91.5 mAh/g after 100 cycles or a capacity retention of 65%. The improved performance is further confirmed by the more stable CE for samples with Al_2O_3 coating. For bare NMC samples, the CE starts to fluctuate remarkably after 25 cycles with a standard deviation as high as 4.5%. In contrast, only a small fluctuation of 1.0% is observed in NMC with 2 nm coating after 50 cycles, with an average CE of 99.0%. Although the cycling performance is not as good as that with a 4.2 V cutoff, the remarkable contrast between samples with and without ALD coating clearly demonstrates the effectiveness of Al_2O_3 passivation.

To understand why the Al_2O_3 coating improves the cycling performance, the protective effect of Al_2O_3 is first examined by cyclic voltammetry of carbon fiber papers (CFPs). Carbon fiber papers (AvCarb MGL190) with 0, 2, and 3 nm were combined with lithium metal counter electrodes and scanned between 2.5 and 4.5 V vs Li/Li+ at 1 mV/s for five cycles (Figure 3A). The anodic current above 4.0 V vs Li/Li+ is
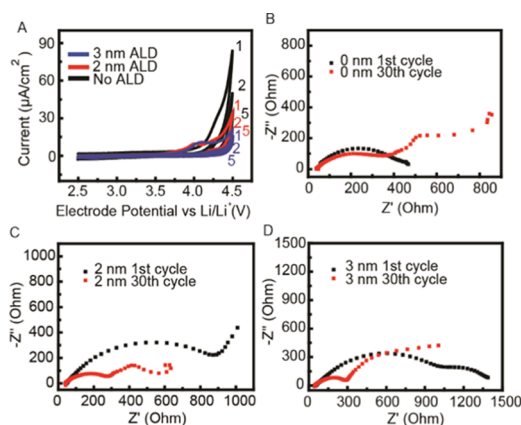
Figure 3. Cyclic voltammetry and electrochemical impedance spectroscopy (EIS) of NMC/PEG/Li cells. (A) Cyclic voltammetry at cycles 1, 2, and 5 for carbon fiber paper with 3, 2, and without Al_2O_3 coating. The scan rate is 1 mV/s. (B) EIS at the 1st cycle and 30th cycle, without Al_2O_3 coating. (C) EIS at the 1st cycle and 30th cycle, with a 2 nm Al_2O_3 coating. (D) EIS at the 1st cycle and 30th cycle, with a 3 nm Al_2O_3 coating.

significantly smaller than that of bare carbon, indicating less oxidation of the PEG electrolyte. For example, in cycle 1, anodic current densities on bare CFP are 13.7, 28.1, and 81.6 $\mu A/cm^2$ at 4.2, 4.3, and 4.5 V, respectively, but reduce to 11.1, 14.1, and 34.3 $\mu A/cm^2$ for CFP with a 2 nm Al_2O_3 coating and to 10.2, 11.2, and 17.9 $\mu A/cm^2$ for CFP with a 3 nm Al_2O_3 coating (Figure S4). Similarly, in cycle 5, while the anodic current density remains at 2.5, 3.5, and 28.1 $\mu A/cm^2$ at 4.2, 4.3, and 4.5 V for bare CFP, the current densities are only 2.6, 3.5, and 15.6 $\mu A/cm^2$ for CFP with 2 nm Al_2O_3 and 2.3, 3.1, and 8.8 $\mu A/cm^2$ for CFP with 2 nm Al_2O_3, respectively, representing a reduction of 40−70% in the oxidation rate (Figure S7). It should be noted that the area for values above is based on the geometric area; so, the true anodic current density normalized to the electrode surface area is significantly lower. A simple estimation based on the electrical double-layer capacitance indicates that the true surface area is about 100 times that of the geometric footprint so that the current densities normalized to the true surface area is 2 orders of magnitude lower (see Supporting Information Note 1).

To better understand how the reduced activity on Al_2O_3-protected surface leads to improved electrochemical performance, electrochemical impedance spectroscopy (EIS) is carried out on bare NMC/Li and 2 nm Al_2O_3-coated NMC/Li cells at 4.2 V. As shown in Figure 3B, when bare NMC is used, the impedance at 0.1 Hz increases from 468 to 896 Ω from cycle 1 to cycle 30, and the higher impedance arises from a significantly longer diffusion tail, indicating that PEG oxidation also affects ionic diffusion in the solid NMC particles, at least the surface layer (Figure S12). On the other side, the impedance at 0.1 Hz of a 2 nm Al_2O_3-coated NMC decreases from 1020 to 620 Ω in Figure 3D, which can be attributed to
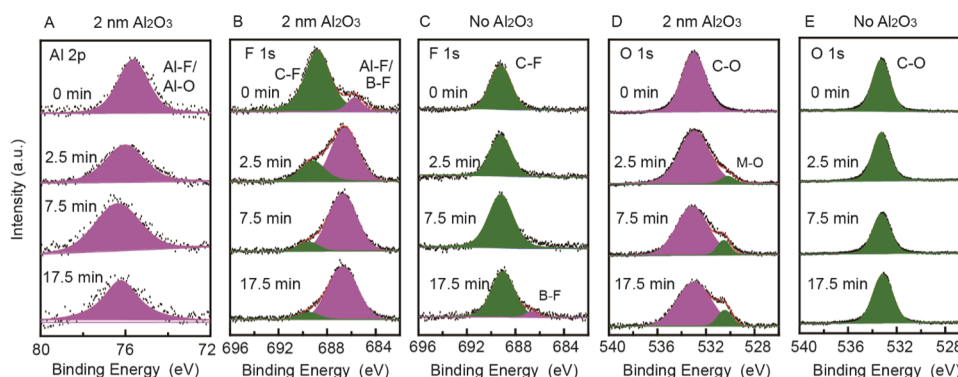
Figure 4. XPS depth profile on the surface of NMC electrodes cycled for 50 times. (A) Al 2p signal on the NMC electrode with a 2 nm Al_2O_3 coating. (B and C) F 1s signal on NMC with a 2 nm Al_2O_3 coating (B) and bare NMC (C). O 1s signal on NMC with a 2 nm Al_2O_3 coating (D) and bare NMC (E). M−O bonds can be assigned to either Ni/Mn/Co or Al−O bonds.

the lower impedance at the lithium anode. As cycling goes on, the repeated deposition of Li will increase the surface area due to increased surface roughness and the formation of mossy lithium. This has been observed in various literatures as reduced overpotential and lower impedance.[35,38] This is further confirmed by our EIS measurement of Li/Li cells with the same electrolyte used in NMC/Li cells in the paper. Hence, even if the impedance from the NMC electrode is steady, the total cell impedance still decreases due to the reduced impedance at the lithium anode (Figure S8), which is the case for 2 and 3 nm Al_2O_3-coated NMCs. This indicates that there is no significant increase in impedance on the cathode side once Al_2O_3 is applied, which stabilizes the interface. For the 3 nm Al_2O_3 coating, even though the impedance decreases from 1391 to 1089 Ω at 0.1 Hz in Figure 3D, confirming that the coating helps stabilize the system, we can see that the impedance is obviously larger than the 2 nm coating. This gives us the idea that the 3 nm coating may be too thick to improve battery performance, especially for power density.

To better understand the protective mechanism chemically, the XPS depth profile of NMC electrodes after 50 cycles is measured. Two kinds of samples are compared, the bare NMC electrode and the NMC electrode with a 2 nm Al_2O_3 coating, which were both rinsed in 1,2-dimethoxyethane (DME) for 15 s and dried before characterizations. Both samples are sputtered for 0, 2.5, 7.5, and 17.5 min to obtain the depth profile. The nominal sputtering speed is 2 nm/min calibrated by Cu; so, nominally, they correspond to depths of 0, 5, 15, and 35 nm, respectively. However, it should be noted that the sputtering rate differs from material to material; so, the depth can only be used as a reference. First, the Al peak is clear on the NMC electrode with a 2 nm Al_2O_3 coating. Al peaks at all depths can be assigned to either Al−O and/or Al−F bonds, which are both known to protect layered oxide cathodes.[39,40] The F 1s peaks are also distinct for two samples. In the sample with 2 nm coating, although the surface signal is dominated by C−F from PVDF at 688.8 eV, the peak at 686.7 eV dominates for 2.5−17.5 min sputtering. This peak can be assigned to Al−F, which is consistent with the results on the Al peak.[40,41] The energy of 686.7 eV aligns with B−F too, which may come from the oxidation of LiBOB.[42] However, the concentration of B−F is unlikely to be high, since B signal is very weak on the NMC surface (Figure S9). On the other hand, the dominant F 1s signal in the bare NMC is the C−F bond from PVDF. No Al−

F or B−F is observed except a small peak at 17.5 min sputtering (Figure 4C).

O and C peaks also unveil important information. For the NMC electrode with 2 nm coating, although the dominant signal is C−O bond in O 1s (Figure 4D) and C 1s peaks (Figure S10), a metal-O peak arises starting from 2.5 min of sputtering (∼5 nm), indicating that the CEI layer is thin.[43,44] In contrast, on the bare NMC electrode, no M−O bond is detected even down to 17.5 min of sputtering (∼35 nm), suggesting a thick layer of CEI, which may block ion transport. The difference in SEI thickness is also supported by the XPS depth profile of Ni/Mn/Co, which shows up clearly after 2.5 min sputtering in the sample with a 2 nm Al_2O_3 coating. On the other side, without Al_2O_3 coating, these transitional metals cannot be detected even after 17.5 min sputtering (Figure S10).[45] C peaks further show that the major compositions of carbon species in CEI are C−O−C (286.6 eV, ether) and C−C/C−H (284.8 eV) in both samples, with a low concentration of C=O centered at 289.2 eV, which may arise from the oxidation of PEG.[42,44,46] The XPS results clearly prove that there are remarkable differences of CEI for samples with Al_2O_3 coating and without coating. The participant of Al in CEI formation alters the surface chemistry and leads to more protective phases, such as AlF_x and BF_x, which slows down PEG oxidation. The thickness of CEI is also smaller, which facilitates ion transport. To examine the stability of the Al_2O_3 coating, the NMC electrode with 2 nm coating after 50 cycles is further characterized by TEM (Figure S11). A clear Al signal is still observed outside the Co layer after cycling. This validates our assumption that the ALD coating layer is effective and stable during cycling.

■ CONCLUSIONS

In conclusion, a 2 nm conformal coating of Al_2O_3 is shown to be effective in remarkably improving the stability of the PEG-based electrolyte with the NMC electrode. When charged to 4.2 V, the initial capacity at C/3 reaches 128.5 mAh/g. It remains at 101.8 mAh/g after 100 cycles and 85.7 mAh/g after 200 cycles. In contrast, the capacity fades fast from 130.1 to 26.3 mAh/g in 40 cycles for NMC electrodes without coating. Cyclic voltammetry and XPS analyses show that the improved stability can be attributed to slower oxidation kinetics of PEG on the NMC surface and the formation of chemically distinct cathode electrolyte interphase. This study opens a new possibility to combine high-energy-density NMC electrode materials with PEO-based electrolyte, which is safer than

conventional carbonate electrolytes. Further optimization, including adjusting salt concentration and nonflammable additives, could further enhance safety, cycle life, and energy density of this battery system.

EXPERIMENTAL SECTION

Material and Characterizations. $LiNi_{1/3}Mn_{1/3}Co_{1/3}O_2$ (NMC) powders were purchased from MSE Supplies LLC and used as received. SUPER C65 carbon black and Kynar 761 PVDF were received from Timcal and Arkema, respectively. LiTFSI was received from Solvay. LiBOB and LiDFOB were received from Gotion Inc. Poly(ethylene glycol) dimethyl ether (M_w = 500) was purchased from Sigma-Aldrich. Lithium metal foil with a thickness of 0.75 mm was purchased from Alfa Aesar. Carbon fiber paper was purchased from Fuel Cell Earth LLC.

HAADF images and elemental mapping were conducted by an FEI TALOS F200X transmission/scanning transmission electron microscope (TEM/STEM). EDS in SEM was performed by a Zeiss Sigma VP SEM equipped with an EDS detector. Surface analysis was performed by a PHI 5500 XPS. Before XPS, the electrodes were removed from coin cells and rinsed by 1,2-dimethoxyethane (DME) for 15 s to remove electrolyte residue. Ignition test was performed by dropping 0.2 mL electrolyte on a glass plate, followed by fire ignition.

Synthesis of Al_2O_3-Coated NMC. The coating of Al_2O_3 was performed in a Cambridge Nanotech Savannah 200 ALD system. The as-coated NMC electrode is placed in the chamber at 100 °C. The trimethyl aluminum and water source were pumped inside alternatively. Each pulse, hold period, and pumping time were 0.03, 5, and 25 s, respectively. The N_2 flow rate is 20 sccm. Nominally, 1, 2, and 3, 2 nm coatings correspond to 10, and 20 and 30 cycles of ALD, respectively.

Electrochemical Characterization. The NMC electrode (~3.0 mg/cm^2 or ~0.4 mAh/cm^2) was prepared by casting a slurry mixture containing 88 wt % NMC, a 5 wt % SUPER C65 conductive carbon, and 7 wt % PVDF in 1-methyl-2-pyrrolidone (NMP). After drying, the electrode was calendared and punched into disks with a diameter of 12 mm and further dried at 110 °C for 3 h. The as-prepared NMC electrode was assembled with a lithium metal anode, a PEG-based electrolyte, and Celgrad separators in a 2032 coin cell.

The galvanostatic cycling was performed by Landt battery testers. Cyclic voltammetry was performed by a Bio-logic VMP3 tester. The cell assembly was done in a glovebox (MBraun LABmaster) filled with argon gas (<1 ppm O_2 and <1 ppm H_2O). The conductivity of the electrolyte was measured in a square quartz cell, where the electrode area is 1 cm^2 and the electrode distance is 1 cm.

ASSOCIATED CONTENT

Ⓢ Supporting Information

The Supporting Information is available free of charge on the ACS Publications website at DOI: 10.1021/acsami.9b04932.

Flammability test of the electrolyte system in this paper; cycling performance of salt concentrations; HAADF image and EDS data of an NMC electrode with a 2 nm Al_2O_3 coating by ALD; conductivity of LiTFSI + LiBOB in PEGDME between 10 and 60 °C; power capabilities with and without ALD coatings; electrochemical performance of Al_2O_3-protected NMC electrodes charge-cycled between 2.8 and 4.25 V vs Li/Li$^+$; electrochemical stability of PEG with NMC; EIS of Li | Li symmetric cells with the electrolyte in this paper; the XPS depth profile of NMC electrode after 50 cycles; XPS surveys of NMC surface; the HAADF image of an NMC electrode with 2 nm Al_2O_3 coating by ALD after cycling and EDS mapping of Al/Co overlapping; EIS simulation with COMSOL for the 1D case of lithium ions diffusion in bare NMC cathode; explanation of the

relations between true surface area and geometric area; and the flash point of PEG with M_w of 500 (PDF)
Flammability test (MP4)

AUTHOR INFORMATION

Corresponding Author
*E-mail: yy2664@columbia.edu.
ORCID Ⓘ
Haowei Zhai: 0000-0002-7030-3563
Qian Cheng: 0000-0001-5510-2977
Yuan Yang: 0000-0003-0264-2640

Author Contributions

‖H.Z., T.G., and B.X. contributed equally to this work.

Author Contributions

The manuscript was written through contributions of all authors. All authors have given approval to the final version of the manuscript.

Notes

The authors declare no competing financial interest.

REFERENCES

(1) Lu, J.; Chen, Z.; Ma, Z.; Pan, F.; Curtiss, L. A.; Amine, K. The role of nanotechnology in the development of battery materials for electric vehicles. *Nat. Nanotechnol.* **2016**, *11*, No. 1031.

(2) Lu, Y.; Tu, Z.; Archer, L. A. Stable lithium electrodeposition in liquid and nanoporous solid electrolytes. *Nat. Mater.* **2014**, *13*, 961−969.

(3) Whittingham, M. S. Lithium Batteries and Cathode Materials. *Chem. Rev.* **2004**, *104*, 4271−4302.

(4) Xu, K. Electrolytes and Interphases in Li-Ion Batteries and Beyond. *Chem. Rev.* **2014**, *114*, 11503−11618.

(5) Naguib, M.; Allu, S.; Simunovic, S.; Li, J.; Wang, H.; Dudney, N. J. Limiting Internal Short-Circuit Damage by Electrode Partition for Impact-Tolerant Li-Ion Batteries. *Joule* **2018**, *2*, 155−167.

(6) Seo, D.-H.; Lee, J.; Urban, A.; Malik, R.; Kang, S.; Ceder, G. The structural and chemical origin of the oxygen redox activity in layered and cation-disordered Li-excess cathode materials. *Nat. Chem.* **2016**, *8*, No. 692.

(7) Gent, W. E.; Li, Y.; Ahn, S.; Lim, J.; Liu, Y.; Wise, A. M.; Gopal, C. B.; Mueller, D. N.; Davis, R.; Weker, J. N.; Park, J.-H.; Doo, S.-K.; Chueh, W. C. Persistent State-of-Charge Heterogeneity in Relaxed, Partially Charged Li1−xNi1/3Co1/3Mn1/3O2 Secondary Particles. *Adv. Mater.* **2016**, *28*, 6631−6638.

(8) Liao, X.; Shi, C.; Wang, T.; Qie, B.; Chen, Y.; Yang, P.; Cheng, Q.; Zhai, H.; Chen, M.; Wang, X.; Chen, X.; Yang, Y. High-Energy-Density Foldable Battery Enabled by Zigzag-Like Design. *Adv. Energy Mater.* **2019**, *9*, No. 1802998.

(9) Qian, G.; Zhu, B.; Liao, X.; Zhai, H.; Srinivasan, A.; Fritz, N. J.; Cheng, Q.; Ning, M.; Qie, B.; Li, Y.; Yuan, S.; Zhu, J.; Chen, X.; Yang, Y. Bioinspired, Spine-Like, Flexible, Rechargeable Lithium-Ion Batteries with High Energy Density. *Adv. Mater.* **2018**, *30*, No. 1704947.

(10) Bachman, J. C.; Muy, S.; Grimaud, A.; Chang, H. H.; Pour, N.; Lux, S. F.; Paschos, O.; Maglia, F.; Lupart, S.; Lamp, P.; Giordano, L.; Shao-Horn, Y. Inorganic Solid-State Electrolytes for Lithium Batteries: Mechanisms and Properties Governing Ion Conduction. *Chem. Rev.* **2016**, *116*, 140−162.

(11) Liu, H.; Wang, X.; Zhou, H.; Lim, H.-D.; Xing, X.; Yan, Q.; Meng, Y. S.; Liu, P. Structure and Solution Dynamics of Lithium Methyl Carbonate as a Protective Layer For Lithium Metal. *ACS Appl. Energy Mater.* **2018**, *1*, 1864−1869.

(12) Tsai, P.-C.; Wen, B.; Wolfman, M.; Choe, M.-J.; Pan, M. S.; Su, L.; Thornton, K.; Cabana, J.; Chiang, Y.-M. Single-particle measurements of electrochemical kinetics in NMC and NCA cathodes for Li-ion batteries. *Energy Environ. Sci.* **2018**, *11*, 860−871.

(13) Mu, L.; Yuan, Q.; Tian, C.; Wei, C.; Zhang, K.; Liu, J.; Pianetta, P.; Doeff, M. M.; Liu, Y.; Lin, F. Propagation topography of redox phase transformations in heterogeneous layered oxide cathode materials. *Nat. Commun.* **2018**, *9*, No. 2810.

(14) Schipper, F.; Erickson, E. M.; Erk, C.; Shin, J.-Y.; Chesneau, F. F.; Aurbach, D. Review—Recent Advances and Remaining Challenges for Lithium Ion Battery Cathodes: I. Nickel-Rich, LiNixCoyMnzO2. *J. Electrochem. Soc.* **2017**, *164*, A6220−A6228.

(15) Ren, D.; Shen, Y.; Yang, Y.; Shen, L.; Levin, B. D. A.; Yu, Y.; Muller, D. A.; Abruña, H. D. Systematic Optimization of Battery Materials: Key Parameter Optimization for the Scalable Synthesis of Uniform, High-Energy, and High Stability LiNi$_{0.6}$Mn$_{0.2}$Co$_{0.2}$O$_2$ Cathode Material for Lithium-Ion Batteries. *ACS Appl. Mater. Interfaces* **2017**, *9*, 35811−35819.

(16) Hess, S.; Wohlfahrt-Mehrens, M.; Wachtler, M. Flammability of Li-Ion Battery Electrolytes: Flash Point and Self-Extinguishing Time Measurements. *J. Electrochem. Soc.* **2015**, *162*, A3084−A3097.

(17) Fan, X.; Chen, L.; Borodin, O.; Ji, X.; Chen, J.; Hou, S.; Deng, T.; Zheng, J.; Yang, C.; Liou, S.-C.; Amine, K.; Xu, K.; Wang, C. Author Correction: Non-flammable electrolyte enables Li-metal batteries with aggressive cathode chemistries. *Nat. Nanotechnol.* **2018**, *13*, 1191.

(18) MacFarlane, D. R.; Tachikawa, N.; Forsyth, M.; Pringle, J. M.; Howlett, P. C.; Elliott, G. D.; Davis, J. H.; Watanabe, M.; Simon, P.; Angell, C. A. Energy applications of ionic liquids. *Energy Environ. Sci.* **2014**, *7*, 232−250.

(19) Zhang, X.; Liu, T.; Zhang, S.; Huang, X.; Xu, B.; Lin, Y.; Xu, B.; Li, L.; Nan, C.-W.; Shen, Y. Synergistic Coupling between Li6.75La3Zr1.75Ta0.25O12 and Poly(vinylidene fluoride) Induces High Ionic Conductivity, Mechanical Strength, and Thermal Stability of Solid Composite Electrolytes. *J. Am. Chem. Soc.* **2017**, *139*, 13779−13785.

(20) Ma, Q.; Zhang, H.; Zhou, C.; Zheng, L.; Cheng, P.; Nie, J.; Feng, W.; Hu, Y.-S.; Li, H.; Huang, X.; Chen, L.; Armand, M.; Zhou, Z. Single Lithium-Ion Conducting Polymer Electrolytes Based on a Super-Delocalized Polyanion. *Angew. Chem., Int. Ed.* **2016**, *55*, 2521−2525.

(21) Duan, H.; Yin, Y.-X.; Zeng, X.-X.; Li, J.-Y.; Shi, J.-L.; Shi, Y.; Wen, R.; Guo, Y.-G.; Wan, L.-J. In-situ plasticized polymer electrolyte with double-network for flexible solid-state lithium-metal batteries. *Energy Storage Mater.* **2018**, *10*, 85−91.

(22) Yao, P.; Zhu, B.; Zhai, H.; Liao, X.; Zhu, Y.; Xu, W.; Cheng, Q.; Jayyosi, C.; Li, Z.; Zhu, J.; Myers, K. M.; Chen, X.; Yang, Y. PVDF/Palygorskite Nanowire Composite Electrolyte for 4 V Rechargeable Lithium Batteries with High Energy Density. *Nano Lett.* **2018**, *18*, 6113−6120.

(23) Meyer, W. H. Polymer electrolytes for lithium-ion batteries. *Adv. Mater.* **1998**, *10*, 439−448.

(24) Manthiram, A.; Yu, X.; Wang, S. Lithium battery chemistries enabled by solid-state electrolytes. *Nat. Rev. Mater.* **2017**, *2*, No. 16103.

(25) Mindemark, J.; Lacey, M. J.; Bowden, T.; Brandell, D. Beyond PEO—Alternative host materials for Li+-conducting solid polymer electrolytes. *Prog. Polym. Sci.* **2018**, *81*, 114−143.

(26) Croce, F.; Appetecchi, G. B.; Persi, L.; Scrosati, B. Nanocomposite polymer electrolytes for lithium batteries. *Nature* **1998**, *394*, 456−458.

(27) Zhang, J.; Zhao, N.; Zhang, M.; Li, Y.; Chu, P. K.; Guo, X.; Di, Z.; Wang, X.; Li, H. Flexible and ion-conducting membrane electrolytes for solid-state lithium batteries: Dispersion of garnet nanoparticles in insulating poly(ethylene oxide). *Nano Energy* **2016**, *28*, 447−454.

(28) Zhai, H.; Xu, P.; Ning, M.; Cheng, Q.; Mandal, J.; Yang, Y. A Flexible Solid Composite Electrolyte with Vertically Aligned and Connected Ion-Conducting Nanoparticles for Lithium Batteries. *Nano Lett.* **2017**, *17*, 3182−3187.

(29) Wang, X.; Zhai, H.; Qie, B.; Cheng, Q.; Li, A.; Borovilas, J.; Xu, B.; Shi, C.; Jin, T.; Liao, X.; Li, Y.; He, X.; Du, S.; Fu, Y.; Dontigny, M.; Zaghib, K.; Yang, Y. Rechargeable solid-state lithium metal batteries with vertically aligned ceramic nanoparticle/polymer composite electrolyte. *Nano Energy* **2019**, *60*, 205−212.

(30) Zheng, H.; Qu, Q.; Zhu, G.; Liu, G.; Battaglia, V. S.; Zheng, H. Quantitative Characterization of the Surface Evolution for LiNi0.5-Co0.2Mn0.3O2/Graphite Cell during Long-Term Cycling. *ACS Appl. Mater. Interfaces* **2017**, *9*, 12445−12452.

(31) Lin, D. C.; Liu, W.; Liu, Y. Y.; Lee, H. R.; Hsu, P. C.; Liu, K.; Cui, Y. High Ionic Conductivity of Composite Solid Polymer Electrolyte via In Situ Synthesis of Monodispersed SiO2 Nanospheres in Poly(ethylene oxide). *Nano Lett.* **2016**, *16*, 459−465.

(32) Shi, Q.; Xue, L.; Qin, D.; Du, B.; Wang, J.; Chen, L. Single ion solid-state composite electrolytes with high electrochemical stability based on a poly(perfluoroalkylsulfonyl)-imide ionene polymer. *J. Mater. Chem. A* **2014**, *2*, 15952−15957.

(33) Radin, M. D.; Hy, S.; Sina, M.; Fang, C.; Liu, H.; Vinckeviciute, J.; Zhang, M.; Whittingham, M. S.; Meng, Y. S.; Van der Ven, A. Narrowing the Gap between Theoretical and Practical Capacities in Li-Ion Layered Oxide Cathode Materials. *Adv. Energy Mater.* **2017**, *7*, No. 1602888.

(34) Ma, J.; Liu, Z.; Chen, B.; Wang, L.; Yue, L.; Liu, H.; Zhang, J.; Liu, Z.; Cui, G. A Strategy to Make High Voltage LiCoO2 Compatible with Poly(ethylene oxide) Electrolyte in All-Solid-State Lithium Ion Batteries. *J. Electrochem. Soc.* **2017**, *164*, A3454−A3461.

(35) Jiao, S.; Zheng, J.; Li, Q.; Li, X.; Engelhard, M. H.; Cao, R.; Zhang, J.-G.; Xu, W. Behavior of Lithium Metal Anodes under Various Capacity Utilization and High Current Density in Lithium Metal Batteries. *Joule* **2018**, *2*, 110−124.

(36) Liu, Y.; Tzeng, Y.-K.; Lin, D.; Pei, A.; Lu, H.; Melosh, N. A.; Shen, Z.-X.; Chu, S.; Cui, Y. An Ultrastrong Double-Layer Nanodiamond Interface for Stable Lithium Metal Anodes. *Joule* **2018**, *2*, 1595−1609.

(37) Zheng, J.; Engelhard, M. H.; Mei, D.; Jiao, S.; Polzin, B. J.; Zhang, J.-G.; Xu, W. Electrolyte additive enabled fast charging and stable cycling lithium metal batteries. *Nat. Energy* **2017**, *2*, No. 17012.

(38) Shi, P.; Zhang, L.; Xiang, H.; Liang, X.; Sun, Y.; Xu, W. Lithium Difluorophosphate as a Dendrite-Suppressing Additive for Lithium Metal Batteries. *ACS Appl. Mater. Interfaces* **2018**, *10*, 22201−22209.

(39) Sun, Y.-K.; Lee, M.-J.; Yoon, C. S.; Hassoun, J.; Amine, K.; Scrosati, B. The Role of AlF3 Coatings in Improving Electrochemical Cycling of Li-Enriched Nickel-Manganese Oxide Electrodes for Li-Ion Batteries. *Adv. Mater.* **2012**, *24*, 1192−1196.

(40) Xie, J.; Sendek, A. D.; Cubuk, E. D.; Zhang, X.; Lu, Z.; Gong, Y.; Wu, T.; Shi, F.; Liu, W.; Reed, E. J.; Cui, Y. Atomic Layer Deposition of Stable LiAlF4 Lithium Ion Conductive Interfacial Layer for Stable Cathode Cycling. *ACS Nano* **2017**, *11*, 7019−7027.

(41) Makarowicz, A.; Bailey, C. L.; Weiher, N.; Kemnitz, E.; Schroeder, S. L. M.; Mukhopadhyay, S.; Wander, A.; Searle, B. G.; Harrison, N. M. Electronic structure of Lewis acid sites on high surface area aluminium fluorides: a combined XPS and ab initio investigation. *Phys. Chem. Chem. Phys.* **2009**, *11*, 5664−5673.

(42) Jiao, S.; Ren, X.; Cao, R.; Engelhard, M. H.; Liu, Y.; Hu, D.; Mei, D.; Zheng, J.; Zhao, W.; Li, Q.; Liu, N.; Adams, B. D.; Ma, C.; Liu, J.; Zhang, J.-G.; Xu, W. Stable cycling of high-voltage lithium metal batteries in ether electrolytes. *Nat. Energy* **2018**, *3*, 739−746.

(43) Fleutot, B.; Martinez, H.; Pecquenard, B.; Ledeuil, J. B.; Levasseur, A.; Gonbeau, D. Surface film morphology (AFM) and chemical features (XPS) of cycled V2O5 thin films in lithium microbatteries. *J. Power Sources* **2008**, *180*, 836−844.

(44) Zhao, W.; Zheng, J.; Zou, L.; Jia, H.; Liu, B.; Wang, H.; Engelhard, M. H.; Wang, C.; Xu, W.; Yang, Y.; Zhang, J.-G. High

Voltage Operation of Ni-Rich NMC Cathodes Enabled by Stable Electrode/Electrolyte Interphases. *Adv. Energy Mater.* **2018**, *8*, No. 1800297.

(45) Bergmann, A.; Martinez-Moreno, E.; Teschner, D.; Chernev, P.; Gliech, M.; de Araújo, J. F.; Reier, T.; Dau, H.; Strasser, P. Reversible amorphization and the catalytically active state of crystalline Co3O4 during oxygen evolution. *Nat. Commun.* **2015**, *6*, No. 8625.

(46) Bodenes, L.; Darwiche, A.; Monconduit, L.; Martinez, H. The Solid Electrolyte Interphase a key parameter of the high performance of Sb in sodium-ion batteries: Comparative X-ray Photoelectron Spectroscopy study of Sb/Na-ion and Sb/Li-ion batteries. *J. Power Sources* **2015**, *273*, 14−24.